MABS
2017, VOL. 9, NO. 1, 43–57
http://dx.doi.org/10.1080/19420862.2016.1236882

Taylor & Francis
Taylor & Francis Group

REPORT

OPEN ACCESS

Stability of isolated antibody-antigen complexes as a predictive tool for selecting toxin neutralizing antibodies

Patricia M. Legler[a], Jaimee R. Compton[b], Martha L. Hale[c], George P. Anderson[a], Mark A. Olson[c], Charles B. Millard[c], and Ellen R. Goldman[a]

[a]US Naval Research Laboratory, Washington, DC, USA; [b]NOVA Research, Inc., Alexandria, VA, USA; [c]US Army Medical Research Institute of Infectious Diseases, Frederick, MD, USA

ABSTRACT

Ricin is an A-B ribosome inactivating protein (RIP) toxin composed of an A-chain subunit (RTA) that contains a catalytic N-glycosidase and a B-chain (RTB) lectin domain that binds cell surface glycans. Ricin exploits retrograde transport to enter into the Golgi and the endoplasmic reticulum, and then dislocates into the cytoplasm where it can reach its substrate, the rRNA. A subset of isolated antibodies (Abs) raised against the RTA subunit protect against ricin intoxication, and RTA-based vaccine immunogens have been shown to provide long-lasting protective immunity against the holotoxin. Anti-RTA Abs are unlikely to cross a membrane and reach the cytoplasm to inhibit the enzymatic activity of the A-chain. Moreover, there is not a strict correlation between the apparent binding affinity (K_a) of anti-RTA Abs and their ability to successfully neutralize ricin toxicity. Some anti-RTA antibodies are toxin-neutralizing, whereas others are not. We hypothesize that neutralizing anti-RTA Abs may interfere selectively with conformational change (s) or partial unfolding required for toxin internalization. To test this hypothesis, we measured the melting temperatures (T_m) of neutralizing single-domain Ab (sdAb)-antigen (Ag) complexes relative to the T_m of the free antigen (T_m-shift = $T_m^{complex} - T_m^{Ag}$), and observed increases in the $T_m^{complex}$ of 9–20 degrees. In contrast, non-neutralizing sdAb-Ag complexes shifted the $T_m^{Complex}$ by only 6–7 degrees. A strong linear correlation ($r^2 = 0.992$) was observed between the magnitude of the T_m-shift and the viability of living cells treated with the sdAb and ricin holotoxin. The T_m-shift of the sdAb-Ag complex provided a quantitative biophysical parameter that could be used to predict and rank-order the toxin-neutralizing activities of Abs. We determined the first structure of an sdAb-RTA1-33/44-198 complex, and examined other sdAb-RTA complexes. We found that neutralizing sdAb bound to regions involved in the early stages of unfolding. These Abs likely interfere with steps preceding or following endocytosis that require conformational changes. This method may have utility for the characterization or rapid screening of other Ab that act to prevent conformational changes or unfolding as part of their mechanism of action.

ARTICLE HISTORY
Received 11 May 2016
Revised 31 August 2016
Accepted 12 September 2016

KEYWORDS
Antibody complex; antibody selection; conformational change; mechanism of action; Tm-shift; toxins; unfolding

Introduction

For antibodies developed to treat or prevent infectious diseases or poisoning by protein toxins, the location of the antibody's (Ab) binding site (epitope) can, in some cases, explain its protective effects. For example, an Ab may bind a toxin or pathogen to block or compete with a cell surface receptor and, thereby, reduce or prevent internalization. There are many cases, however, in which the mechanism of action (MOA) of an Ab is not obvious. For toxins, as well as viruses, Abs recognizing the same antigen can be segregated into 2 categories, neutralizing and non-neutralizing, suggesting that some Abs exert additional effects beyond simple binding. Understanding how Ab-mediated toxin neutralization occurs is significant because it can lead to improved toxin-neutralizing Ab-based diagnostics, engineered vaccines, and new small molecule therapeutic strategies.[1,2]

The assessment of the protective effects of Abs traditionally has relied upon dissociation constants (K_d),[3] cell-based assays, and animal studies.[4] Epitopes are categorized as protective or non-protective and the assignment of the epitope to either category is empirically determined. In some cases, non-protective "decoy" epitopes can be found adjacent to protective epitopes, and so the location of an epitope alone is not used to determine if an Ab is protective or non-protective. Even Abs that competitively bind to overlapping epitopes can still differ in their toxin-neutralizing activities.[4] A simple biophysical measurement that can functionally distinguish between a highly protective neutralizing Ab versus a moderate or weakly neutralizing Ab would thus be useful for identifying the different types of Abs elicited by vaccination. Without a biophysical parameter, the selection of a therapeutic Ab or the combinatorial formulation of an Ab cocktail relies on trial and error, requiring a large number of cell-based assays and in some cases animal studies[5,6] to determine the most effective combinations. For highly toxic Select Agents,[7] a biophysical method that uses a toxoid also may reduce the need and associated

CONTACT Patricia M. Legler patricia.legler@nrl.navy.mil; plegler2@gmail.com Naval Research Laboratory, 4555 Overlook Ave, Washington, DC 20375.
Supplemental data for this article can be accessed on the publisher's website.

costs for experiments conducted under biosafety level-2/3 (BSL2/3) containment.

Research and development of improved therapeutics for ricin intoxication is ongoing.[8,9] Ricin is a ribosome inactivating protein (RIP) toxin. Its A-chain (RTA) catalyzes the depurination of A4324 in the α-sarcin/ricin GAGA tetra loop of the 28S rRNA.[10] The B-chain (RTB) is a lectin that binds galactose residues on the cell surface. Since RTA is a highly efficient catalyst, only a few internalized RTA molecules are required to inactivate all of the ribosomes within a target cell.[11] The depurination of the rRNA leads to inhibition of protein synthesis, apoptosis and ultimately cell death.[12]

RTA enters the cytosol by retrograde transport.[13,14] After endosomal uptake RIPs can be destroyed in the lysosome or transported in early endosomes to the trans-Golgi network and then to the endoplasmic reticulum (ER).[9,14,15,16] To reach the cytosol, RTA exploits the ER-associated protein degradation (ERAD) pathway.[17] Unfolded proteins in the ER are normally transported into the cytosol for ubiquitination followed by degradation by the proteasome. A small fraction of RTA in the ER dislocates into the cytoplasm and refolds to a catalytically active enzyme in the cytosol.[18]

Several anti-RTA Abs elicited by RTA subunit vaccine immunogens are known to protect against intoxication in animals. These immunogens do not contain the RTB lectin domain. Two RTA subunit vaccines, RiVax[19] and RTA1-33/44-198 (also called RVEC),[20] have been tested as vaccine immunogens in Phase 1 clinical studies (Fig. 1). RTA1-33/44-198 was shown to protect mice against 10 LD_{50} of ricin delivered intranasally.[21] Additionally, the neutralizing activities of single-domain antibodies (sdAb) and antigen (Ag)-binding fragments (Fab) in cell-based assays are independent of the Fc domain.[22]

It has been suggested that anti-RTA Abs may work by direct inhibition of RTA enzymatic activity; however, an anti-RTA Ab able to inhibit the enzymatic activity was found to be non-neutralizing.[4] Moreover, Abs that enter into the cell during endocytosis are compartmentally separated from ribosomes in the cytosol by a membrane, and likely do not prevent or interfere with RTA substrate binding within the cytoplasm to exert their protective effects. So how do these anti-RTA Abs protect against ricin intoxication?

We hypothesize that some toxin-neutralizing Abs may block the unfolding of RTA or prevent a conformational change within RTA and thereby inhibit intoxication. RTA's ability to unfold and refold is central to its currently accepted mechanism of target cell entry and intoxication.[23] Like Ab binding, the nucleation of protein unfolding is thought to occur at specific locations in the 3 dimensional structure.[24] Identification and conformational restriction of these regions has been exploited for the stabilization of enzymes and proteins.[24,25,26,27] The melting temperature (T_m) of a protein reflects a protein's intrinsic propensity to unfold. Thermal denaturation of a protein or protein-protein complex can be monitored by circular dichroism (CD), the mid-point of the transition yields the apparent T_m. Thermodynamic analysis of folding-unfolding requires that the 2 states coexist at the T_m with equal populations ($\Delta G = 0$).[28] Since the unfolding of RTA yields a non-equilibrium condition by way of aggregation, the ΔG at the T_m is not zero. Both thermal and chemical denaturation of RTA is an irreversible process.[29] Thus, the measured T_m values of RTA and its complexes are denoted as apparent T_m values, and should not be interpreted as a thermodynamic measure of stability. Nevertheless, the apparent T_m's can still yield useful information regarding the relative stability of these proteins and protein-protein complexes. Both CD and differential scanning calorimetry are label-free methods that have

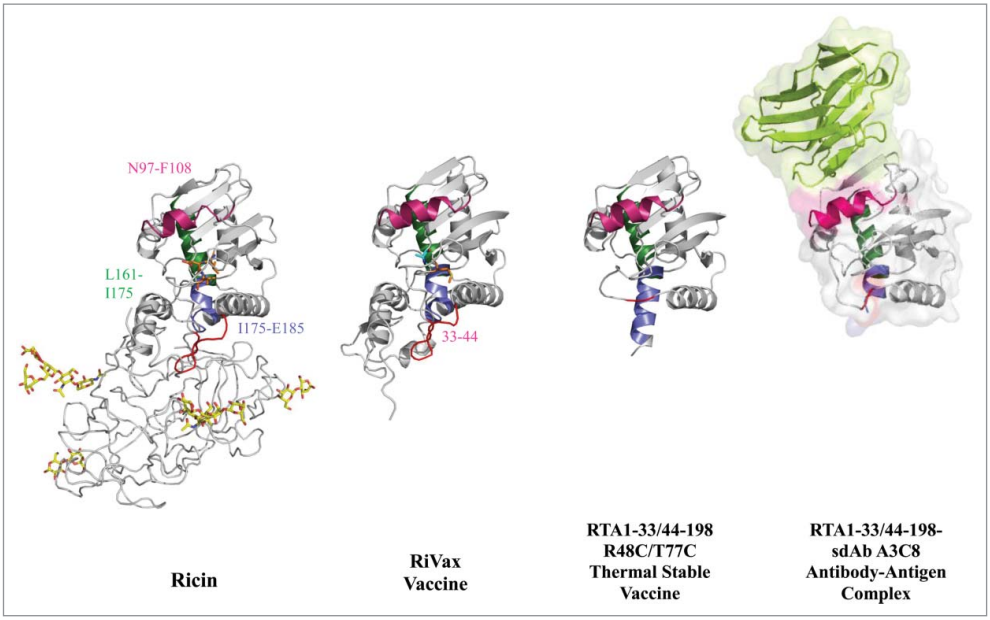

Figure 1. Ricin is an A-B toxin: the catalytic A-chain (RTA) is shown in ribbon, and the RTB lectin domain in worm (PDB 2AAI).[69] Glycans are shown in stick. The RiVax vaccine is an inactive RTA variant containing 2 mutations, V76M and Y80A (PDB 3SRP).[70] RTA1-33/44-198 R48C/T77C is a thermostabilized RTA variant created by truncating RTA at residue 198, removing a loop between residues 34–43, and incorporating a disulfide (R48C/T77C) (PDB 3LC9).[30] The structure of RTA1-33/44-198 in complex with the toxin-neutralizing sdAb A3C8 (PDB 5SV4) is shown on the right. The epitope (N97-F108) bound by the most potent neutralizing anti-ricin antibody (UNIVAX 70/138, also known as R70[71]) is shown in hot pink. The epitope of sdAb A3C8 overlaps with the immunodominant UNIVAX epitope.[72] The immunodominant human B-cell epitope identified by Castelletti et al.[73] (L161-I175) is shown in green, and a T-cell epitope is shown in blue.[74]

been used to measure the T_m of proteins, protein-protein complexes, and protein-small molecule complexes in solution. The T_m can be used to examine the stabilizing effects of conformationally restrictive mutations or, in this case, conformationally restrictive Ab binding.

We previously incorporated disulfide bonds within specific regions of RTA predicted to be involved in the early stages of unfolding based partly upon *in silico* predictions. The elevation of the T_m of a protein can be practically useful during manufacturing and for the development of long shelf-life vaccine immunogens,[30] or for the development of field-expedient protein-based assay reagents that do not require refrigeration.[31] Incorporation of a disulfide bond at 2 sites within RTA led to 2 engineered immunogens with enhanced stability as judged by a higher apparent T_m.[30] Disulfides incorporated at 7 other sites had little or no effect on the T_m. Our findings with engineered disulfides suggest that specific structural regions within RTA may play a preferential role in controlling overall protein stability. Likewise, earlier work showed that the introduction of an intrachain disulfide bond within RTA (S215C/M255C) could interfere with ricin toxicity.[32] We hypothesized that, if partial unfolding of RTA is necessary for toxin internalization, toxin-neutralizing Abs may act like our engineered disulfides by locally stabilizing the folded structure and, thereby, interfering with intoxication.

We propose here that the magnitude of the T_m-shift induced by an Ab may be useful in predicting the toxin-neutralizing activities of anti-RTA Abs that prevent conformational change or unfolding. To test this hypothesis, we measured the T_m of RTA and compared it with the T_m of RTA in complex with a set of previously identified neutralizing and non-neutralizing sdAb[33,34,22,35,36] at low pH (to mimic the endosomal environment, pH 4.5) or at pH 7.4 (to mimic the extracellular environment). We found that the magnitude of the T_m shift induced by the Ab was highly correlated with the level of protection in cell-based assays. These results suggest a potential MOA for anti-RTA neutralizing Abs, and identify a simple biophysical parameter that may be useful in conjunction with cell-based assays for quantitatively assessing and comparing other protective Ab or small molecules as experimental therapeutics.

Results

Structure of the A3C8 single-domain antibody

The A3C8 sdAb was first crystallized. Data collection and refinement statistics are shown in Table 1. A3C8 was found to be monomeric using a calibrated gel-filtration column (Table 2). The structure of the A3C8 sdAb (PDB 5SV4) was used to solve the structure of the sdAb-RTA1-33/44-198 complex by molecular replacement.

Structure of the A3C8:RTA1-33/44-198 complex

Previously, we crystallized 2 thermostabilized variants of RTA1-33/44-198 containing disulfide bonds (Fig. 1);[30] however, we were not able to crystallize the parent protein, RTA1-33/44-198, alone. RTA1-33/44-198 and its variants contain a deletion of loop residues 34–43; these hydrophobic loop residues pack with the C-terminal 199–267 residues (Fig. S1). The removal of residues 34–43 and 199–267 was previously shown to increase the T_m by 8 degrees compared with RTA.[21,37]

Co-crystallization of RTA1-33/44-198 with sdAb A3C~8 enabled us to solve the first structure of the original RTA1-33/44-198 variant and examine the conformation of the sdAb-bound antigen. When sdAb-bound RTA1-33/44-198 was compared with the disulfide bonded variants (PDB 3MK9 and 3LC9),[30] conformational differences were observed in 3 regions: residues 33–52; residues 131–136 and residues 182–188 (Fig. S2). The differences in residues 33–52 are likely due to the disulfide bonds that were incorporated at R48C/T77C and V49C/E99C. In the sdAb A3C8:RTA1-33/44-198 complex, the conformation of the loop residues 131–136 was more similar to that of RTA in the ricin holotoxin (PDB 2AAI), than to the conformation found in the disulfide-bonded variants (PDB 3LC9, 4IMV, and 3MK9).[30,21] In the structures of the disulfide variants, the conformation of loop residues 131–136 found in RTA (PDB 1J1M)[38] would clash with an adjacent molecule at the crystal packing interface. We had previously shown that the B-factors of residues 131–136 were higher in the disulfide-bonded variants compared with RTA, and that the density for the loop was poor, suggesting static or dynamic disorder of these residues.[30] In the A3C8:RTA1-33/44-198 complex (PDB 5SV3), these residues also were involved in a crystal packing interface, but had well-defined density while

Table 1. X-ray crystallography data collection and refinement statistics.

	sdAb A3C8	A3C8:RTA1-33/44-198 Complex
PDB	5SV4	5SV3
Space group	P2(1)2(1)2(1)	P2(1)2(1)2
Unit Cell Dimensions (Å)	35.88, 44.40, 143.77	35.88, 117.76, 130.43
Wavelength (Å)	1.54	1.54
Resolution Range (Å)[a]	47.92–2.70 (2.80–2.70)	65.22–2.73 (2.83–2.73)
Unique Reflections	6,823 (689)	15,475 (1,536)
R_{sym}[b]	0.166 (0.445)	0.187 (0.454)
$I/\sigma I$	12.2 (3.5)	11.9 (4.5)
Completeness	100.0 (100.0)	99.9 (100.0)
Redundancy	11.5 (8.2)	14.0 (14.2)
Refinement Statistics:		
Resolution (Å)	47.92–2.70	65.22–2.73
No. of reflections	6,455	14,603
R_{factor}[c]	0.201	0.228
R_{free}[d]	0.246 (5%)[b]	0.267 (5%)[b]
Number of Atoms:		
Protein	1922	4538
Solvent	60	78
Other	10	10
Average B-factors (Å^2)		
Protein	18.1 (A), 36.7 (B)	29.2(A), 22.9(B), 22.0(C), 32.5(D)
Solvent	18.1	32.1
R.m.s.d. from ideal geometry:		
Bond lengths (Å)	0.010	0.007
Bond angles (degrees)	1.482	1.17
Ramachandran plot		
Most favored regions (%)	93.6%	93.0%
Additional allowed regions (%)	6.4%	7.0%
Generously allowed regions (%)	0.0%	0.0%
Disallowed regions (%)	0.0%	0.0%

[a]Values in parentheses are for the outer most data shell
[b]R_{free} for test set and size of test set as % total reflections in parentheses.

Table 2. Apparent T_m values of SdAb, RTA, RTA1-33/44-198, and their complexes in 1x PBS pH 4.5 or 7.4. Gel-filtration columns were calibrated, and elution volumes are shown for the free proteins and their complexes. The MW has been calculated based upon the protein sequence.

Protein	Type of Antibody	K_d (M)	Apparent T_m (°C)	ΔT_m (°C)	pH	Wavelength (nm)		Elution Volume (mL)	Calculated MW (kDa)
Ricin A-Chain Constructs									
RTA	—	—	52.2 ± 0.1	—	4.5	222	G75	11.0	30.112
RTA	—	—	51.6 ± 0.7	—	7.4	222	G200	16.1	30.112
RTA1-33/44-198	—	—	57.6 ± 0.5	—	4.5	214	G75	13.0	22.595
RTA1-33/44-198	—	—	55.5 ± 0.1	—	7.4	222	G200	16.3	22.595
Anti-RTA Antibodies									
A3C8	Neutralizing	—	66.2 ± 0.4	—	4.5	207, 222	G75	12.3	15.063
A3C8	Neutralizing	—	70.7 ± 0.1	—	7.4	222	G200	16.6	15.063
C8	Neutralizing	—	58.1 ± 0.5	—	4.5	207, 222	G75	12.5	13.576
C8	Neutralizing	—	60.5 ± 0.3	—	7.4	207, 222	G200	16.8	13.576
D10	Neutralizing	—	66.8 ± 0.4	—	7.4	207, 222	G200	17.0	13.999
D12f	Neutralizing	—	78.8 ± 0.4	—	7.4	222	G200	16.6	14.224
H1W12V	Non-Neutralizing	—	67.0 ± 0.4	—	7.4	207	G200	16.6	14.766
C10neg	Non-Neutralizing	—	77.9 ± 1.2	—	7.4	207	G75	13.2	13.941
F6	Non-Neutralizing	—	76.3 ± 0.4	—	7.4	207	G75	12.5	14.942
E1	(Non-Neutralizing)[a]	—	66.4 ± 0.5	—	7.4	207, 222	G75	12.7	14.723
RTA1-33/44-198-Antibody Complexes									
RTA1-33/44-198:A3C8	Neutralizing	1.48 E-08	66.6 ± 0.5	9.0	4.5	214	G75	11.1	37.658
RTA1-33/44-198:A3C8	Neutralizing	7.22 E-10	68.3 ± 0.2	12.8	7.4	222	G200	14.8	37.658
RTA1-33/44-198:A3C8	Neutralizing	7.22 E-10	69.3 ± 0.5	13.8	7.4	222	G75	10.8	37.658
RTA1-33/44-198:C8	Neutralizing	1.55 E-08	64.2 ± 0.1	6.6	4.5	214	G75	11.2	36.171
RTA1-33/44-198:C8	Neutralizing	1.40 E-10	69.87 ± 0.03	14.4	7.4	222	G75	10.9	36.171
RTA1-33/44-198:D10	Neutralizing	1.75 E-10	71.1 ± 0.2	15.6	7.4	222	G75	10.9	36.594
RTA1-33/44-198:D12f	Neutralizing	1.16 E-10	75.0 ± 0.3	19.5	7.4	222	G75	10.9	36.819
RTA1-33/44-198:H1W12V	Non-Neutralizing	—	No Complex	—	7.4	—	G75	12.1	37.361
RTA1-33/44-198:C10neg	Non-Neutralizing	—	No Complex	—	7.4	—	G75	12.2,13.4	36.536
RTA1-33/44-198:F6	Non-Neutralizing	3.13E-08	59.9 ± 0.2	4.4	7.4	222	G75	11.1	37.537
RTA1-33/44-198:E1	(Non-Neutralizing)[a]	3.58 E-09	69.6 ± 0.3	14.1	7.4	222	G75	10.8	37.318
RTA-Antibody Complexes									
RTA:A3C8	Neutralizing	4.32 E-09	58.3 ± 0.3	6.1	4.5	222	G75	9.7	45.175
RTA:A3C8	Neutralizing	4.6 E-10	60.3 ± 0.7	8.7	7.4	222	G75	10.5	45.175
RTA:A3C8	Neutralizing	4.6 E-10	61.0 ± 1.1	9.4	7.4	222	G200	14.5	45.175
RTA:C8	Neutralizing	5.98 E-09	58.9 ± 0.2	6.7	4.5	214	G75	9.8	43.688
RTA:C8	Neutralizing	1.63 E-10	71.9 ± 0.3	20.3	7.4	222	G200	14.8	43.688
RTA:D10	Neutralizing	1.44 E-10	66.4 ± 0.4	14.8	7.4	222	G200	14.8	44.094
RTA:D12f	Neutralizing	2.27 E-11	67.7 ± 0.6	16.1	7.4	222	G200	14.8	44.336
RTA:H1W12V	Non-Neutralizing	5.18 E-10	57.2 ± 0.6	5.6	7.4	222	G200	14.6	44.878
RTA:C10neg	Non-Neutralizing	—	No Complex	—	7.4	222	G75	11.1, 13.1	43.851
RTA:F6	Non-Neutralizing	6.04 E-09	57.1 ± 0.4	5.5	7.4	222	G75	10.4	45.054
RTA:E1	(Non-Neutralizing)[a]	1.25 E-09	58.4 ± 0.3	6.8	7.4	222	G75	10.5	44.835

[a]This antibody is reported to be a non-neutralizing, but has also been reported to compete with a neutralizing antibody

residues 188–198 (near the 33–44 loop) appeared disordered. The C-terminal domain packs with the 131–136 loop residues and residues 182–188. The C-terminal domain and residues 182–188 contact RTB (Fig. 1, Fig. S1, S2). The conformation of these loop residues may be stabilized by the C-terminal domain residues 199–267 or by sdAb A3C8 binding. However, a structure of the free RTA1-33/44-198 is still needed to confirm this effect.

Effects of the Q98A, Q112A and R114A mutations on sdAb A3C8 binding

The epitope recognized by A3C8 was initially identified using the crystal structure of the complex. The epitope then was confirmed by site-directed mutagenesis, Western blotting, and surface plasmon resonance (SPR; Fig. 2).

A C-terminal His-tagged sdAb and anti-His-tag IgG were used to detect RTA and its variants in Western blot analysis. Antigens were separated by SDS-PAGE. Based upon the crystal structure (PDB 5SV3), 3 residues were selected for mutation: Q98A, Q112A, and R114A. Other previously characterized disulfide-bonded RTA1-33/44-198 variants[30,21] were included: R48C/T77C; V49C/E99C; A90C/V111C; R125C/A165C; E138C/P143C; N141C/I192C; and R48C/T77C/D75N. A total of 10 RTA1-33/44-198 variants were examined in addition to recombinant RTA and RTA purified from *Ricinus communis*. Staining was observed for all of the RTA1-33/44-198 variants (0.5 μg per lane) with the exception of R114A, indicating that R114A mutation disrupted sdAb A3C8 binding. The Q112A variant showed slightly reduced staining.

SPR was used to examine changes in affinity to the epitope since multiple contacts were observed between the antibody and antigen (Table 3). For sdAb A3C8, the R114A mutation led to the most significant increase in the dissociation constant (49-fold higher K_d), and the Q112A mutation lead to a ~2-fold higher K_d compared with RTA1-33/44-198.

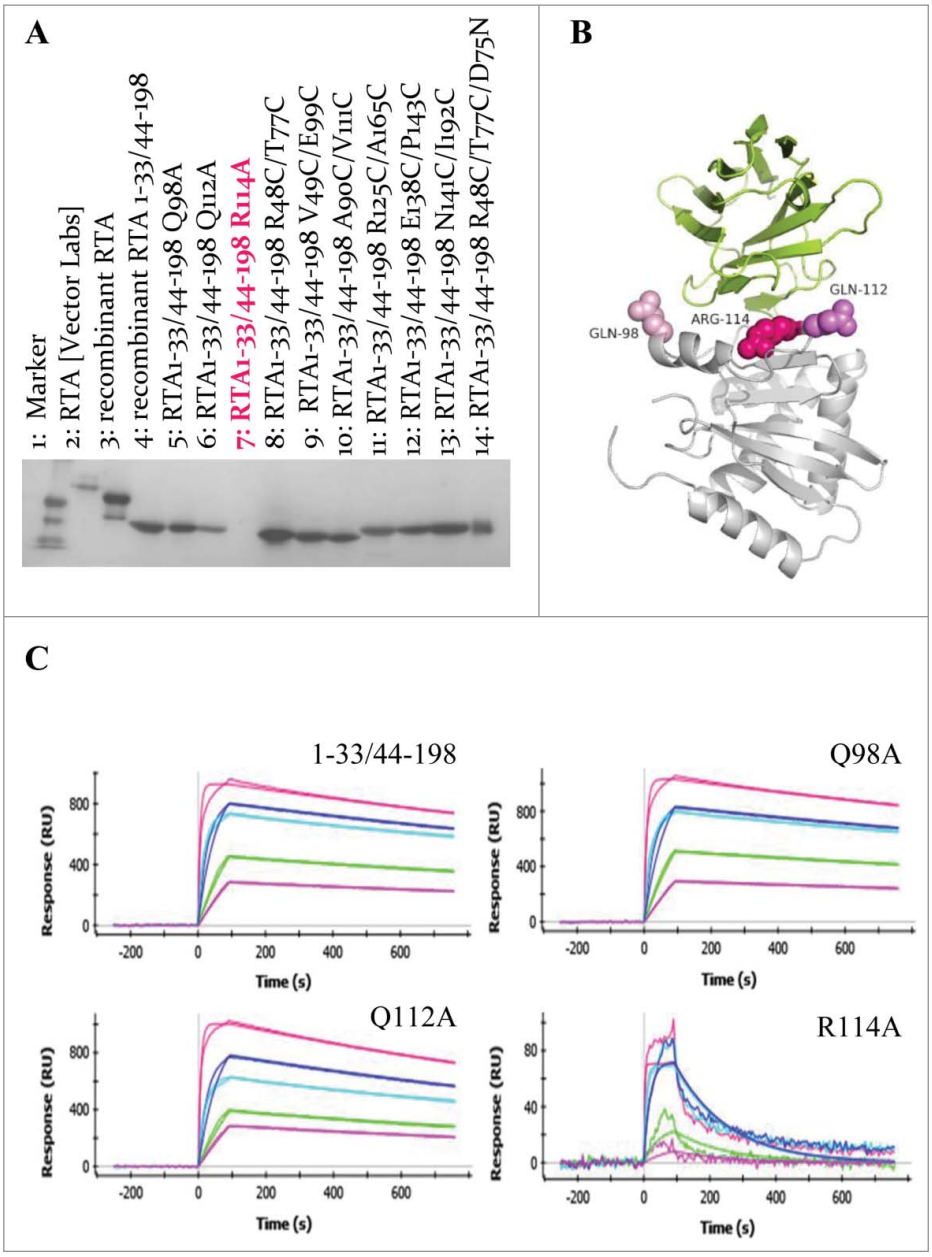

Figure 2. SdAb A3C8 epitope identification. (A) Western analysis to identify residues important for Ab binding using mutants of RTA.[30,21] His-tagged sdAb A3C8 was used as the primary Ab. A mouse anti-His-tag Ab was used as the secondary Ab, and an anti-mouse alkaline phosphatase linked Ab was used for detection. (B) SdAb A3C8 Ab-Ag interface (PDB 5SV3) showing the location of 3 mutations (pink spheres): Q98A, Q112A, and R114A. (C) Apparent Ab on and off rates measured by SPR for RTA1-33/44-198 and the Q98A, Q112A, and R114A variants. Tight binding by sdAb A3C8 was not observed to the R114A variant by SPR or Western analysis.

Ab binding to the denatured RTA was consistent with binding to a linear epitope (Fig. 2A). However, binding to an N-terminally biotinylated-peptide that contains residues H94-T116 (^{94}HPDNQEDAEAITHLFTDVQNRYT^{116}) and the UNIVAX R70 epitope (underlined) was not detectable by SPR, suggesting that the Ab may make an important contact to residues outside of this region. A3C8 carries the same complementarity-determining region (CDR) sequences as C8, but has a different framework. A3C8 bound less well to RTA than C8 (Table 3) suggesting that the framework residues may favor particular side-chain conformations of CDR residues involved in binding or alter the mobility of the CDRs.

Epitope mapping of other anti-ricin sdAb: D12f, D10, E1, F6, C10neg and H1W12V

We also identified the general locations of the epitopes of the other sdAb tested. The K_d values measured for RTA, RiVax, RTA1-33/44-198, and the 3 variants are summarized in Table 3. The structure of the D10:RTA complex had been previously determined,[22] and the Q98A, Q112A and R114A mutations did not have significant effects on binding affinity consistent with the structure (Fig. 3E). Like sdAb A3C8, the D12f sdAb had markedly reduced affinity (41-fold higher K_d) for the R114A variant, suggesting that the epitopes of the neutralizing D12f and A3C8 sdAb overlapped (*n.b.* sdAb A3C8 and C8 contain the same CDRs).

Table 3. Dissociation constants measured by SPR for sdAb and RTA and its variants. Binding of the A3C8 antibody was disrupted by the R114A mutation in both Western blots and SPR experiments. DB denotes 'disrupted binding': the response units (y-axis) for these mutants were <10% of the parent protein and the on and off rates could not be accurately determined for the mutant. Dashes indicate that the change in K_d was < 2-fold from the parent protein. The disruption mutations were used to identify the general locations of the epitopes recognized by these Abs.

	sdAb	k_{on} (1/M*sec)	k_{off} (1/sec)	K_d (M)	Fold Difference in K_d (RTA vs. Mutants)	Fold Difference in K_d (RTA1-33/44-198 vs. Mutants)
RTA	A3C8	700,000	0.000263	4.6×10^{-10}	—	
RiVax	A3C8	974,000	0.000205	2.11×10^{-10}	—	
RTA 1-33/44-198	A3C8	552,000	0.000346	6.27×10^{-10}	—	—
RTA 1-33/44-198, Q98A	A3C8	437,000	0.000306	7.01×10^{-10}		—
RTA 1-33/44-198, Q112A	A3C8	483,000	0.000484	1.00×10^{-9}		—
RTA 1-33/44-198, R114A	A3C8	531,000	0.0164	3.09×10^{-8}		49-fold
RTA	C8	1,320,000	0.000215	1.63×10^{-10}	—	
RiVax	C8	1,800,000	0.000205	1.14×10^{-10}	—	
RTA 1-33/44-198	C8	1,090,000	0.000152	1.40×10^{-10}	—	—
RTA 1-33/44-198, Q98A	C8	1,210,000	0.000228	1.89×10^{-10}		—
RTA 1-33/44-198, Q112A	C8	836,000	0.000224	2.68×10^{-10}		—
RTA 1-33/44-198, R114A	C8	DB	DB			≥100-fold
RTA	D10	396,000	0.0000570	1.44×10^{-10}	—	
RiVax	D10	539,000	0.0000979	1.82×10^{-10}	—	
RTA 1-33/44-198	D10	416,000	0.0000729	1.75×10^{-10}	—	—
RTA 1-33/44-198, Q98A	D10	439,000	0.0000688	1.57×10^{-10}		—
RTA 1-33/44-198, Q112A	D10	500,000	0.0000915	1.83×10^{-10}		—
RTA 1-33/44-198, R114A	D10	732,000	0.000183	2.50×10^{-10}		—
RTA	D12f	418,000	0.00000948	2.27×10^{-11}	—	
RiVax	D12f	476,000	0.0000149	3.12×10^{-11}	—	
RTA 1-33/44-198	D12f	350,000	0.0000407	1.16×10^{-10}	5-fold	—
RTA 1-33/44-198, Q98A	D12f	388,000	0.0000286	7.38×10^{-11}		—
RTA 1-33/44-198, Q112A	D12f	447,000	0.0000307	6.88×10^{-11}		—
RTA 1-33/44-198, R114A	D12f	680,000	0.00324	4.77×10^{-9}		41-fold
RTA	F6	197,000	0.00119	6.04×10^{-9}	—	
RiVax	F6	167,000	0.00128	7.65×10^{-9}	—	
RTA 1-33/44-198	F6	358,000	0.0112	3.13×10^{-8}	5-fold	—
RTA 1-33/44-198, Q98A	F6	313,000	0.0116	3.70×10^{-8}		—
RTA 1-33/44-198, Q112A	F6	371,000	0.0128	3.45×10^{-8}		—
RTA 1-33/44-198, R114A	F6	DB	DB			≥100-fold
RTA	E1	188,000	0.000235	1.25×10^{-9}	—	
RiVax	E1	194,000	0.000194	1.00×10^{-9}	—	
RTA 1-33/44-198	E1	296,000	0.00106	3.58×10^{-9}	3-fold	—
RTA 1-33/44-198, Q98A	E1	279,000	0.00105	3.76×10^{-9}		—
RTA 1-33/44-198, Q112A	E1	323,000	0.00118	3.67×10^{-9}		—
RTA 1-33/44-198, R114A	E1	414,000	0.00173	4.18×10^{-9}		—
RTA	H1W12V	8,620,000	0.00447	5.18×10^{-10}	—	
RiVax	H1W12V	100,000,000	0.0408	4.08×10^{-10}	—	
RTA 1-33/44-198	H1W12V	DB	DB		≥100-fold	—
RTA 1-33/44-198, Q98A	H1W12V	DB	DB			≥100-fold
RTA 1-33/44-198, Q112A	H1W12V	DB	DB			≥100-fold
RTA 1-33/44-198, R114A	H1W12V	DB	DB			≥100-fold

The H1W12V Ab, which is non-neutralizing, had significantly reduced affinity for RTA1-33/44-198 (>100-fold higher K_d) and the 3 RTA1-33/44-198 variants, suggesting that the epitope is within the C-terminal domain residues, 199–267, or within the loop (residues 34–43). The loop (residues 33–44) packs with the C-terminal domain[37] (Fig. S1). The weakly neutralizing G11 sdAb, for which a structure is known, is an example of an sdAb that can bind the C-terminal domain[22] (Fig. 3E). The non-neutralizing Ab, C10neg, did not bind to RTA alone. This Ab is thought to bind to regions of both the A- and B-chains of ricin. The C-terminal domain of RTA packs with RTB (Fig. 1). The F6 sdAb, which also is a non-neutralizing Ab, had slightly reduced binding affinity to RTA1-33/44-198 (5-fold), and showed no significant binding to the R114A variant, suggesting that the F6 epitope may be near that of sdAb A3C8. The epitope of F6 may be near the epitope recognized by the non-neutralizing sdAbs A7 and G12.[22] The E1 sdAb, which is also non-neutralizing, was not significantly affected by the Q98A, Q112A or R114A mutations or by the C-terminal domain truncation.

Analysis of linear regression models and comparison of mean values

We assembled a set of neutralizing and non-neutralizing Abs. The sdAb was classified as neutralizing if >50% cell viability was obtained in the cell-based assays using the specified concentrations of ricin and sdAb. In cell-based assays using the ricin holotoxin, 50% cell viability corresponded to sdAb with IC_{50} values ≤ 80 nM. The sdAb were classified as non-neutralizing if <50% cell viability was obtained or the Ab had IC_{50} values > 80 nM. For the 4 non-neutralizing sdAb used in this study, the IC_{50} values exceeded the highest concentration of ricin tested (5 μM) (Table 4). The A3C8 sdAb is an engineered thermostabilized variant containing the CDRs of the C8 sdAb and the framework regions of a thermostable anti-SEB (Staphylococcal enterotoxin B) Ab called A3 ($T_m = 85°C$).[39] The A3C8

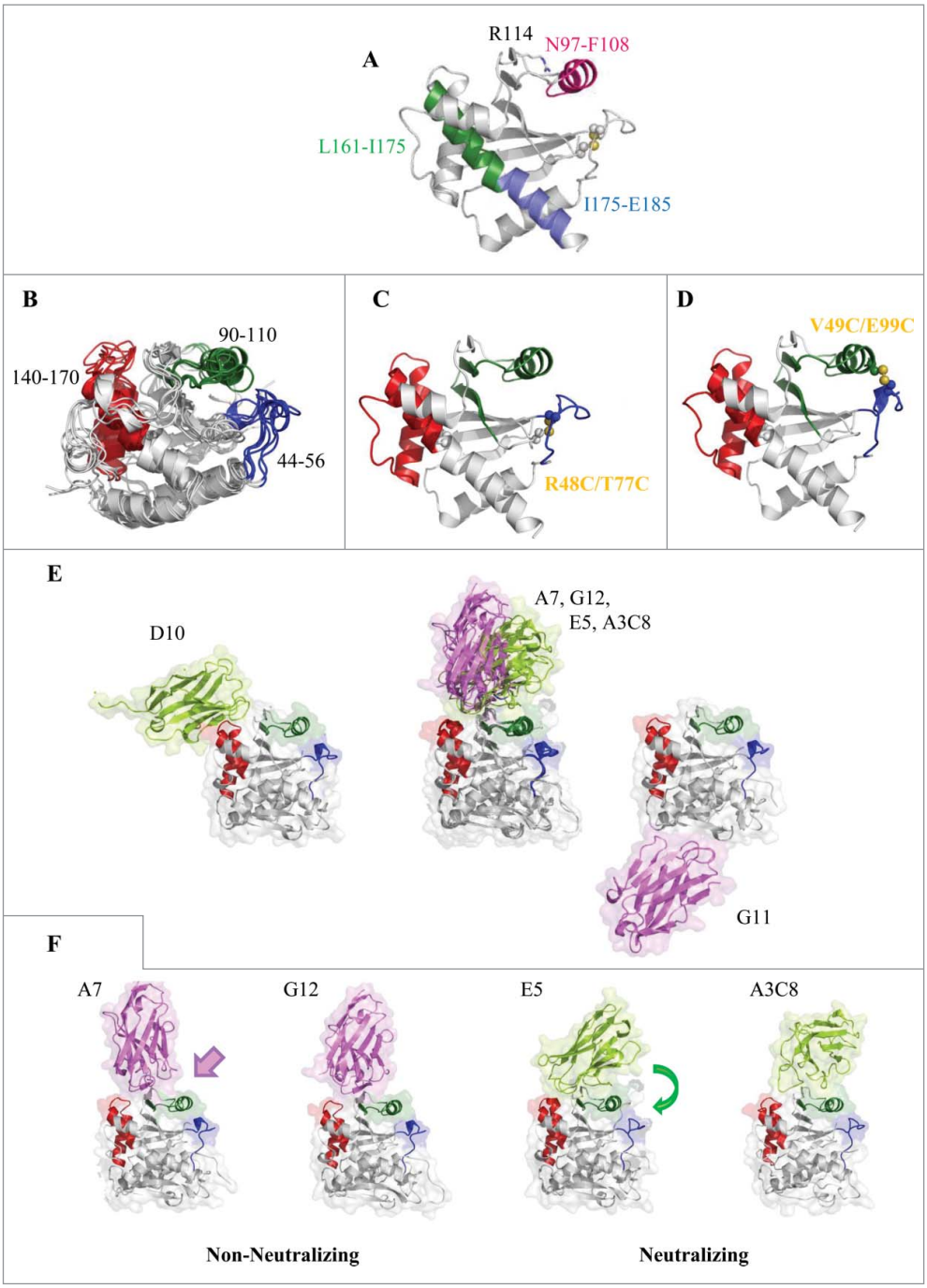

Figure 3. (A) The B-cell and T-cell epitopes are shown for reference in this view and are colored as in Fig. 1. (B) Five conformations of modeled RTA1-33/44-198 from replica-exchange molecular dynamics simulations culled at 298 K with the previously identified regions involved in the early stages of unfolding are shown in blue, red and green.[30] The 2 immunodominant B-cell epitopes are located within 2 of these regions. (C) Locations of 2 disulfide bonds previously engineered into these regions to thermostabilize the protein. A residue within the blue region was anchored to the core of the protein in the R48C/T77C variant (PDB 3LC9).[30] (D) Two residues in the blue and green regions were anchored to one another in the V49C/E99C variant (PDB 3MK9).[30] The R48C/T77C and V49C/E99C mutations both increased the T_m of the protein by 5 degrees relative to the parent construct RTA1-33/44-198, and by 9 degrees relative to RTA. (E) Comparison of the A3C8 structure (PDB 5SV3) with 5 other sdAb-RTA complex structures previously reported by Rudolph, et al.[22] Neutralizing anti-ricin Abs were found bound to 2 of the 3 regions involved in the early stages of unfolding. The strongly neutralizing Abs (lime green) bound to the red (residues 140–170) or green (residues 90–110) regions of RTA. Weakly neutralizing and non-neutralizing sdAb are shown in pink. A weakly neutralizing Ab (G11, PDB 4LHJ) bound to a region distant from the red, green and blue regions of RTA and had an IC_{50}[22] which was estimated to be higher than that of sdAb A3C8. (F) Four neutralizing and non-neutralizing Abs appeared to bind to a similar region, however the most potent toxin-neutralizing Abs (lime, E5 PDB 4LGP and A3C8 PDB 5SV3) were found to pack with the green helical region (residues 90–110) of RTA, while the non-neutralizing ("decoy") and weakly neutralizing Abs (pink, PDB 4LGS, 4LHQ) left this helix exposed to solvent. Similarly, the D10 sdAb packed with the helix-turn-helix motif (red, residues 140–170) more than the non-neutralizing "decoy" Abs A7 and G12.

sdAb has a T_m that is 10°C higher than that of C8. The A3C8 variant binds the same epitope as C8, but with 3-fold lower affinity than C8 (Table 2). This difference allowed us to examine the effects of K_d. The binding of D12f was affected by the R114A mutation and its epitope likely overlaps with that of C8 and A3C8. SdAb D10 is also a neutralizing Ab; its epitope is known and differs from that of A3C8, C8, and D12f (Fig. 3). For non-neutralizing Abs, we selected H1W12V, C10neg, F6

Table 4. Neutralizing activities of anti-RTA sdAb in cell-based assays and in cell-free translation assays. Results are expressed as the percent of viable control cells ([experimental/untreated control] × 100) and are the average of 3 experiments. The standard deviations are shown. Antibodies yielding <50% viable cells were not considered to be 'toxin-neutralizing'. For cell-free translation assays results are expressed as percent control ([experimental/untreated control] × 100) and are the average of 3 experiments; standard deviations are shown.

Antibody	Cell Viability (%)	IC_{50} (nM)	Ribosomal Activity in a Cell-free Translation Assay (%)	T_m Shift (°C)	K_d (M)	T_m Antibody (°C)
Neutralizing						
C8	70 ± 4	40	49 ± 3	20.3	1.63 E-10	60.5
D12f	66 ± 4	30	60 ± 4	16.1	2.27 E-11	78.8
D10	63 ± 4	53	57 ± 2	14.8	1.44 E-10	66.8
A3C8	54 ± 2	80	44 ± 4	8.7	4.6 E-10	70.7
Non-Neutralizing						
H1W12V	18 ± 4	>5000	27 ± 4	5.6	5.18 E-10	67
C10neg	15 ± 3	>5000	14 ± 3	—[a]	—[a]	77.9
F6	12 ± 3	>5000	24 ± 2	5.5	6.04 E-09	76.3
E1	7 ± 3	>5000	14 ± 4	6.8	1.25 E-09	66.4
Controls						
Cells (No Toxin)	100 ± 3		100 ± 4	—	—	—
PBS	5 ± 2		5 ± 3	—	—	—

[a]Antibody recognizes RTA/RTB and does not form a stable complex with RTA alone.

and E1. The E1 and H1W12V sdAbs recognize an epitope within the C-terminal domain residues 199–267, and the C10neg sdAb recognizes both RTA and RTB. To find correlations between the toxin-neutralizing activities of the sdAb and various biophysical parameters, we performed linear regression analysis and examined the r^2-values (Fig. 5). We also compared the difference between the mean values of the biophysical parameters relative to the variation in the sample data, and p-values were calculated from T-values. In our cell viability assays, all of the sdAb concentrations were above the K_d values (i.e., stoichiometric binding regime). All experiments were carried out in triplicate, and the averages and standard deviations are summarized in Table 4. Melting temperatures were measured by monitoring changes in secondary structure as the temperature was raised using a CD spectrometer (Table 2, Fig. 4).

Cell viability vs. percent inhibition of translation

We observed a correlation between cell viability vs. percent inhibition of translation ($r^2 = 0.912$). The T-value was 6.5747 and p-value 0.000297; however, the correlation is not necessarily related to the MOA of anti-RTA Abs (Fig. 5A). This coincidence has been noted by others,[4] and may be due to the location of active site and substrate binding residues within the neutralizing epitopes[40] (Fig. S3). Residues 90–110 contain the UNIVAX R70 epitope (N97-F108) and form a portion of the substrate binding site. Similarly, the B-cell epitope (L161-I175) forms a portion of the substrate binding site. However, while ricin can enter into the Golgi, ER and cytoplasm,[41,42] the anti-ricin Abs likely do not unfold and translocate into the cytoplasm via retrograde transport (i.e., ERAD system) to inhibit the enzymatic activity of RTA. Antibodies are typically separated from their cargo and recycled via the neonatal Fc receptor. Notably, a non-neutralizing anti-RTA antibody known as mAb RAC23 that can inhibit RTA's enzymatic activity, but fails to protect in cell-based assays, has been reported.[4,43,44] RAC23 actually enhanced the toxicity of ricin in a mouse model.[4] The neutralizing anti-RTA mAb called RAC18 led to the accumulation of ricin at the cell surface, suggesting that this neutralizing anti-RTA Ab halts an early step(s) in retrograde transport,[41] rather than RTA substrate binding or catalysis in the cytoplasm. Comparison of sdAb A3C8 with C8 showed that both sdAb comparably inhibited cell-free translation, and that inhibition in cell-free translation could not distinguish between the 2 sdAb. So, while neutralizing and non-neutralizing Abs could be distinguished from one another in this graph, a MOA involving the inhibition of the enzymatic activity in the cytoplasm by an Ab is not supported by Abs such as RAC23.[41]

T_m shift vs. cell viability

A strong correlation between cell viability and the magnitude of the T_m shift was observed for neutralizing Abs and yielded a coefficient of determination $r^2 = 0.992$ and a linear relationship

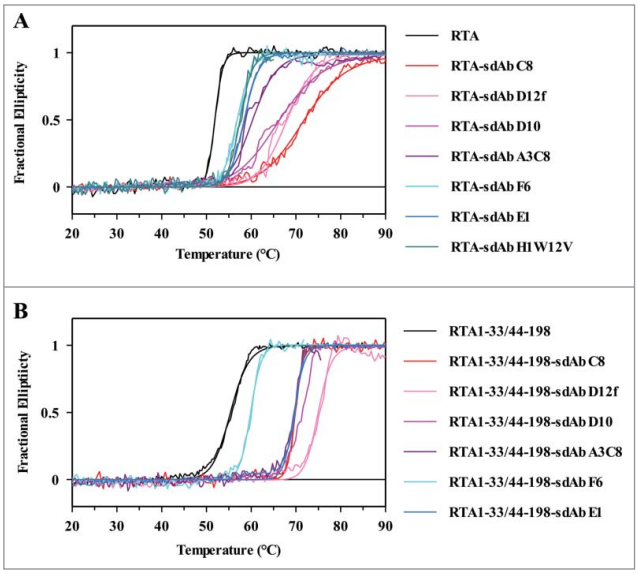

Figure 4. Toxin-neutralizing antibodies (shades of red, pink, and purple) shift the apparent T_m of the Ab-Ag complex more significantly than do non-neutralizing (shades of blue) Abs. Thermal denaturation in 1x PBS pH 7.4 was monitored using a CD spectrometer fitted with a Peltier temperature control unit. In (A), the thermal denaturation of the RTA-sdAb complexes are shown. In (B), the effect is perturbed when RTA is substituted by RTA1-33/44-198 in the sdAb-Ag complexes. RTA1-33/44-198 is a variant of RTA that has a reduced propensity to unfold under thermal stress (higher apparent T_m).

with a positive slope of 0.65 ± 0.05 ($\Delta T_m/\Delta$% cell viability) and a negative y-intercept (−26 ± 3); the x-intercept corresponded to 40% cell viability and was near the 50% cutoff for neutralizing vs. non-neutralizing Abs (Fig. 5B). A similar correlation was obtained with IC_{50} values measured by cell-based assays and T_m shifts ($r^2 = 0.846$) (Fig. 5D). The ranges on the x- and y-axes were relatively large compared with the other parameters, and the points were well dispersed along the line. Excluding the engineered A3C8 sdAb, the mean values of the T_m-shifts for the neutralizing vs. non-neutralizing Abs were compared and produced a T-value = 6.48 and a p-value of 0.00146 (one-tailed), showing that the magnitude of the T_m-shifts for the neutralizing Abs was significantly higher than those of the non-neutralizing Abs. With the inclusion of A3C8, the T-value was 3.15 and the p-value was 0.0127 (one-tailed), showing that the mean value of the T_m-shifts obtained for the neutralizing Abs still was significantly different from that of the non-neutralizing Abs. Thus, the magnitude of the T_m-shift could be used to distinguish between neutralizing and non-neutralizing Abs. Notably, the magnitude of the T_m-shift rank-ordered the sdAb in the same manner as the cell-based assay data.

The apparent T_m values of the Ab-Ag complexes containing RTA (residues 1–267, 30 kDa) were well correlated with the ability of the sdAb to protect cells from intoxication during exposure to the 59 kDa A-B ricin toxin. However, a much poorer correlation was observed as the stability of the ricin A-chain antigen was altered (i.e., RTA1-33/44-198 was used in place of RTA), suggesting that a property of the Ab-Ag complexes had been perturbed (Fig. 4). No significant correlation between cell viability and T_m-shift was observed with the thermostabilized RTA1-33/44-198 variant ($r^2 = 0.2836$). RTA1-33/44-198 had been engineered to have a reduced propensity to unfold, and lacks the C-terminal domain and a loop formed by residues 34–43 that pack with the C-terminal domain. The C-terminal domain packs with RTB[37] (Fig. 1, Fig. S2).

T_m shift vs. percent inhibition of translation

Analysis of all of the data points for both neutralizing and non-neutralizing sdAb. This resulted in only a weak correlation ($r^2 = 0.667$) between these parameters (Table 4).

T_m shift vs. K_d

For neutralizing and non-neutralizing Abs, no correlation between K_d and T_m shift was observed ($r^2 = 0.295$) (Table 4). The T_m reflects a protein's propensity to unfold. This result suggested that the location(s) at which the sdAb bind, rather than their binding affinity, may affect RTA's propensity to unfold. Previously, we had identified 3 regions that became disordered during the early stages of unfolding as the protein was heated *in silico*[30] (Fig. 3B). We showed that we could elevate the T_m of RTA1-33/44-198 by disulfide bonding these regions to the core of the protein or to one another. The T_m values of 2 disulfide-bonded RTA1-33/44-198 variants were increased by 5 degrees (Fig. 3C, 3D). Disulfide bonds introduced at other locations did not significantly increase the T_m of the RTA1-33/44-198 construct.[30] Other groups have empirically identified regions that affect unfolding by mutagenesis alone.[27] In regards to Ab binding, residues within these 3 loop regions were found to be engaged by neutralizing Abs (Fig. 3E). Non-neutralizing Abs recognizing so-called "decoy" epitopes adjacent to these regions did not pack well with the 90–110 or 140–170 residues compared with the neutralizing A3C8 (PDB 5SV3) and E5 (PDB 4LGP)[22] sdAb. The exposed surface area of these 3 regions differed in the neutralizing vs. non-neutralizing Ab complexes (Fig. 3F).

Cell viability vs. K_d

For RTA and anti-RTA Abs, the K_d was not a strongly predictive parameter of neutralizing activity (Fig. 5C). However, neutralizing activity was affected by K_d in some cases (e.g., C8 vs. A3C8). The K_d value has been shown to be a predictive parameter for other antibodies,[3] and the correlation between K_d and protection may largely depend upon the MOA of the protective Ab. From competition experiments we know that D12f and C8 bind the same epitope or overlapping epitopes (Table 3). The K_d values for D12f and C8 differ by a factor of 10; however, the percentage of viable cells obtained for the weaker binding C8 sdAb was higher than that of the tighter binding D12f sdAb. The trend was reversed for A3C8 and C8. A3C8 and C8 have the same CDR sequences and Kd values that differ by 3-fold. A lower percentage of viable cells was obtained with the weaker binding A3C8 sdAb compared with the tighter binding C8 sdAb. The p-value confirmed that K_d alone could not be used to distinguish between neutralizing and non-neutralizing anti-RTA sdAb. For the neutralizing and non-neutralizing sdAb, the T-value was −1.6554 and the p-value was 0.07937 (one tailed). The spread and overlap are shown in (Fig. 5C).

T_m of the antibody vs. T_m of the complex

Thermostabilized Abs have been developed as robust affinity reagents for refrigeration-free use.[45,46,39] Thus, we examined whether a high T_m Ab would be advantageous in preventing the unfolding of its cognate antigen as temperature was varied. Interestingly, there was no advantage in using a thermostabilized sdAb. This was most clearly demonstrated with sdAb A3C8 and C8. SdAb A3C8 has a T_m that is ~10 degrees higher than that of sdAb C8. The T_m of the A3C8:RTA complex was ~11 degrees lower than the T_m of the C8:RTA complex. The T_m of the Ab did not correlate with the T_m of the RTA-sdAb complex for neutralizing ($r^2 = 0.064$) or non-neutralizing Abs ($r^2 = 0.361$). The Tm values of the free neutralizing and non-neutralizing Abs were similar (p-value = 0.30), while the Tm values of the Ab-Ag complexes differed (Tables 2, 4).

Effect of pH on the sdAb-RTA complexes

After the A-B ricin toxin is endocytosed, RTA is separated from RTB shortly (~minutes) after internalization.[47] Endosomes play an important role in transporting and sorting molecules to different compartments in the cell.[48] Endosomes acidify as they transit through the cell and Abs release their antigens. Crystal structures of RTA have been determined at both low (pH 4.2)[49] and high (pH 8.9)[50] pH indicating that RTA can remain stably folded in both acidic

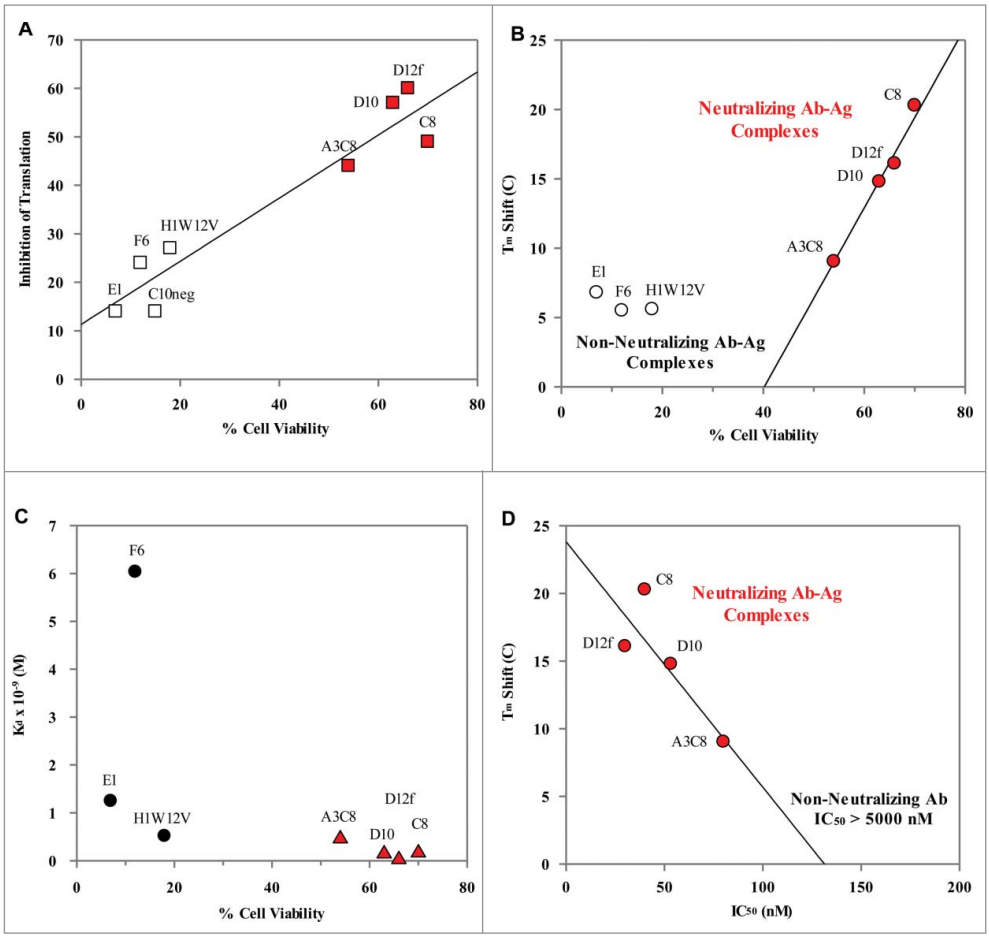

Figure 5. Correlations between the T_m-shift, % Inhibition of translation, and K_d with cell viability or IC_{50}. (A) Comparison of the % inhibition of translation by neutralizing (n = 4) and non-neutralizing (n = 4) sdAbs yielded a p-value = 0.0003 for a one-tailed hypothesis (T-value = 6.57). The significance threshold was set at 0.05. A linear fit of all of the data points yielded an r^2-value = 0.910. While the difference was significant, a mechanism for Ab-bound RTA entry into the cytoplasm has not been reported, and an Ab which inhibits RTA's enzymatic activity but does not neutralize cytotoxicity has been reported.[4] (B) Comparison of the T_m-shifts induced by neutralizing (n = 4) and non-neutralizing sdAb (n = 3) yielded a p-value = 0.0127 (T-value = 3.15) for a one-tailed hypothesis. The significance threshold was set at 0.05. For the neutralizing sdAb, a linear fit of the T_m-shifts vs. the % cell viability (n = 4) yielded an r^2-value = 0.992 suggesting a strong correlation between the 2 parameters. Notably, when the stability of the RTA antigen was altered (i.e. RTA 1-33/44-198 was used in place of RTA), the correlation between the T_m-shift and the % cell viability was lost (r^2-value = 0.18) suggesting that a property of the Ag-Ab complexes had been perturbed. (C) Comparison of the K_d vs. cell viability using a 2-tailed hypothesis yielded a p-value = 0.16 indicating that the K_d does not significantly correlate with the effects of the sdAb in cell-based assays. The significance threshold was set at 0.05. (D) The T_m-shift also correlated well with the IC_{50} (nM) values obtained from cell based assays.

and basic conditions. To determine if the neutralizing sdAb still could remain bound and reduce RTA's propensity to unfold at low pH, we measured the Tm values of the purified RTA-sdAb complexes at pH 4.5 to mimic the endosomal environment. At pH 4.5 micromolar concentrations of the RTA:A3C8, RTA:C8, RTA1-33/44-198:A3C8 and RTA1-33/44-198:C8 complexes still could be purified by gel-filtration. The K_d values were ~10–110-fold higher at pH 4.5 than at pH 7.4 (Table 2). The shifts in the T_m of the RTA:A3C8 vs. RTA:C8 complexes still were detectable at pH 4.5 (6.1 degrees and 6.7 degrees, respectively) (Table 2). The elution volumes differed for the sdAb, RTA, and the RTA-sdAb complexes, and were additional confirmation that the complexes had been purified (Fig. S4). For sdAb C8, the magnitude of the T_m shift decreased significantly from 20.3 °C (pH 7.4) to 6.7 °C (pH 4.5), suggesting that the sdAb may predominantly exert their effects at neutral pH, but can remain bound to the antigen at low pH. The stability of the sdAb-RTA complexes at both pH may be important to their MOA.

Discussion

For ribosome inactivating proteins (RIPs) prior attempts to inhibit the enzymatic activity of the A-chains have had limited success, and no post-exposure small molecule therapeutics are available to reverse the effects of intoxication. For most enzymes, in vitro kinetic methods as well as thermal shift assays and other binding assays have been developed to facilitate the separation of potent from weakly inhibitory compounds. Comparatively few cell-free assays are available for screening therapeutic anti-toxin Abs. Improved cloning, expression, and selection methods also have increased the number of Ab-based therapies undergoing expensive human clinical trials, but there is a shortage of validated cost-effective methods that rank-order different Abs. Expensive and time-consuming cell-based assays and in vivo studies involving pathogens or Select Agent toxins must be performed to differentiate among neutralizing and non-neutralizing Abs, followed by in vitro measurements of Kd values, but the K_d does not necessarily predict biological or clinical efficacy. For some antigens and Abs, the K_d is predictive

of the protective effects of an Ab,[3] but for others no correlation is observed. The correlation between K_d and protection may be indicative of a specific MOA that may not be generally applicable to protein toxins such as ricin, which must undergo conformational changes or partial unfolding in order to enter a cell.

Conformational changes occur in a variety of biochemical processes. Abs that stabilize one conformational state over another may be common.[51,52,53,54,55] The MOA may be rarely recognized since, in these cases, no notable conformational changes would be observed upon Ab binding and alternate conformations of the antigen may elude structural determination. As this study shows, knowledge of the general location of an epitope derived from structures of antibody-bound RTA complexes is not sufficient to predict the neutralizing effects of an Abs, and "decoy epitopes" recognized by non-neutralizing Ab can be found adjacent to epitopes recognized by neutralizing Ab. For toxins, as well as viruses, neutralizing and non-neutralizing Abs recognizing the same antigen can be identified using cell-based assays, indicating that the 2 types of Abs are exerting different effects on the antigen that are protective to the cell.[53,52,4,54] How and where an Ab binds appears to be significant.

Conformationally restrictive mutations in some but not all locations in a 3-dimensional fold can affect the T_m of a protein.[30,24,27] Here, we used a structure-guided biophysical approach to examine Abs that appear to conformationally restrict 3 regions of the RTA protein that become disordered during the early stages of unfolding. Neutralizing sdAb packed with 2 of these regions, while non-neutralizing sdAb bound to regions adjacent to or away from these regions. Here we found that the magnitude of the T_m-shift induced by an Ab bound to its Ag reflected how well an Ab was able to neutralize the ricin toxin in cell-based assays, and that the correlation could be perturbed by altering the stability of either the Ag or Ab as we have done here (i.e., (A3C8 vs. C8) or (RTA vs. RTA1-33/44-198). Interestingly, the largest effect on the T_m-shift arose from sdAb C8, which recognizes a region of RTA containing an immunodominant epitope (N97-F108); its effects on the T_m-shift suggest that this RTA epitope may have functional significance.

Deciding which anti-toxin Abs are the most protective has always been empirically determined using cell-based assays or in vivo studies. This has been primarily due to the lack of a physical parameter that correlates with protection. By examining a set of neutralizing and non-neutralizing sdAbs, we found that the K_d of an Ab-Ag complex was not a discriminating feature of a neutralizing antibody. In fact, the difference in the Kd values of the neutralizing and non-neutralizing antibodies was not statistically significant for anti-RTA Abs. While further studies are warranted to determine if the T_m-shift of an Ab-Ag complex is generally useful for evaluating neutralizing Abs against other foreign proteins, we found that the T_m-shift rank-ordered the toxin-neutralizing Abs without the use of cell-based assays. These results indicate a potential MOA for anti-RTA Abs, and provide a predictive cell-free parameter. This MOA may also apply to Abs that inhibit viral fusion since envelope proteins also undergo conformational changes that are required for viral entry (e.g., influenza hemagglutinin).

As Abs now dominate the biologic therapeutics pipeline, methods that rapidly and quantitatively assess which Abs are more protective than others are of immense value. Understanding of the MOA of Abs may affect how we select and assemble Abs into therapeutic cocktails. Our results suggest that the measurement of the apparent T_m-shift induced by an antibody may be a useful cell-free method to quantify additive or synergistic effects by combinations of Abs. Moreover, using CD to measure the T_m-shift provides a label-free method that has relatively few limitations and can be applied to Abs recognizing linear or conformational epitopes.

Materials and methods

Materials. Q Sepharose, SP Sepharose, Superdex G-200 10/300 GL column, Superdex G-75 10/300 GL column, and PD-10 columns were purchased from GE Healthcare Life Sciences (Piscataway, NJ). General chemicals were purchased from Sigma (St. Louis, MO) or Fisher Scientific (Pittsburgh, PA). *E. coli* BL-21(DE3) cells were purchased from Invitrogen/Life Technologies (Grand Island, NY). BugBuster® Protein Extraction Reagent and TBST buffer was obtained from Millipore (Billerica, MA). SDS-PAGE gels and gel buffers were purchased from Thermo Fisher Scientific Inc. (Rockford, IL). RTA isolated from *Ricinus communis* was purchased from Vector Labs (L-1190, Burlingame, CA). Novagen's mouse anti-His-tag Ab (#70796) was obtained from Millipore (Billerica, MA). Western Blue® stabilized substrate for alkaline phosphatase (AP) and anti-mouse IgG (S3841), Cell Titer 96 reagent, luciferase mRNA, and luciferin substrate were obtained from Promega (Madison, WI). The ammonium sulfate grid screen for crystallization were obtained from Hampton Research (Aliso Viejo, CA).

Cloning of constructs

The sdAb sequences utilized in this work were derived from the variable domain of heavy chain Abs naturally produced by immunized llamas (C8, D12f, H1W12V, C10neg)[33,35] or immunized alpacas (D10, F6, E1).[57] The cloning of sdAb A3, an anti-SEB Ab with a high T_m (T_m = 85°C),[58,39] was previously described and similar methods were used to construct the other sdAb clones. To construct the engineered A3C8 sdAb variant, the CDRs of the anti-RTA sdAb C8 were transferred into the framework regions of sdAb A3 to produce the thermostabilized A3C8 sdAb.[59] Two pet22 constructs of A3C8 were prepared for periplasmic expression— a C-terminal His-tagged plasmid and a tag-free construct (referred to as A3C8stop). The protein sequences are shown in the Suppl. Information.

Protein expression and purification of sdAb

The His-tagged sdAb were periplasmically expressed and purified using the methods previously described in George et al.[39]

Protein expression and purification of RTA and RTA1-33/44-198 and its variants

RTA and RTA1-33/44-198 were purified as previously described.[30] Briefly, *E.coli* BL-21(DE3) were grown in LB media supplemented with Kanamycin (50 μg/ml) at 37°C. Cultures at a cell density of 0.8–1.0 OD_{600} were induced by addition of IPTG (0.2 mM) and grown at 17°C for 18–20 hours before

collection by centrifugation. Cell pellets were resuspended in lysis buffer (50 mM sodium phosphate buffer, pH 7.3, 2 mM EDTA, 30% BugBuster®) and sonicated, 30 seconds on/30 seconds off, for a total of 2 minutes. The lysate was clarified by centrifugation at 20,000 × g for 30 min at 4°C. The supernatant was applied to a Q Sepharose column equilibrated with 50 mM sodium phosphate buffer, 2 mM EDTA, pH 7.3, and the protein was collected in the flow through. Fractions containing the protein were combined and dialyzed overnight at 4°C against 1 L of 50 mM MES, 2 mM EDTA (pH 5.5 for RTA and pH 6.4 for RTA1-33/44-198). Dialyzed protein was loaded onto a SP Sepharose column equilibrated with 50 mM MES, 2 mM EDTA pH 5.5 for RTA and pH 6.4 for RTA1-33/44-198. Protein was eluted from the column using a 0–250 mM sodium chloride gradient and analyzed using SDS-PAGE. The fractions containing a single band on SDS-PAGE gels were combined, dialyzed into 50% glycerol, and stored at −20°C.

Preparation and purification of the RTA:sdAb complexes

RTA:sdAb complexes were prepared by incubating RTA or RTA1-33/44-198 with a 10% molar excess (1:1.1 molar ratio) of each sdAb at 4° C for >17 hours. The concentration of RTA or RTA1-33/44-198 in 0.5 mL was determined by UV-vis using calculated extinction coefficients, $\varepsilon = 26{,}000\ M^{-1}cm^{-1}$ or $\varepsilon = 18{,}005\ M^{-1}cm^{-1}$, respectively. The calculated extinction coefficients for each sdAb were the following: $36{,}565\ M^{-1}cm^{-1}$ for C10neg; 23,045 for H1W12V and F6; and $21{,}555\ M^{-1}cm^{-1}$ for the remaining sdAbs. Each complex was applied to a Superdex G-75 or G-200 gel-filtration column (as appropriate) equilibrated in 1x phosphate-buffered saline (PBS) pH 4.5 or pH 7.4 to separate the formed complex from excess sdAb. To verify the formation of each complex, each column was calibrated using 3 molecular weight (MW) standards: albumin (66,000 Da); carbonic anhydrase (29,000 Da); and cytochrome C (12,400 Da). Calibration curves for each column at pH 4.5 or pH 7.4 were made using a log-linear plot of molecular weight (kDa) vs. elution volume (mL) and fitting the points to a single exponential decay equation using Grafit 5.0 (Erithricus Software Ltd. West Sussex, UK). The MWs of each complex were calculated from the elution volumes and the protein sequence for comparison and confirmation of complex purification.

Circular dichroism and thermal denaturation curves

Thermal denaturation (2°C/min) of RTA, RTA1-33/44-198, the sdAbs, or their complexes, was monitored using a Jasco 810 Circular Dichroism (CD) spectropolarimeter fitted with a Peltier temperature controller. Concentrations of protein solutions (0.2 mg/ml in PBS, pH 4.5 or pH 7.4) were determined by UV-vis using the appropriate calculated extinction coefficient. Melting curves were measured between 10–95°C by monitoring the change in ellipticity at 207, 214, or 222 nm. The apparent melting temperature (T_m) was determined from a 4 parameter fit of data. The three T_m values were averaged and standard deviations (SD) were calculated.

Western analysis of site-directed mutants

Proteins were first separated by SDS-PAGE using an 8–16% gradient gel. Equal amounts of RTA, RTA1-33/44-198, or their variants were loaded (5 μg/lane). RTA isolated from ricin (glycosylated) was used as a control. The proteins in the gel were transferred to nitrocellulose and blocked for 1 h using 1x TBST containing 5% (w/v) dry milk. The primary Ab was incubated in 1x TBST and 5% dry milk for 17 hours at 4°C. The blot was washed 3 times with 1x TBST between subsequent Ab incubations (1 h incubation at 22 ± 3°C) and then developed. SdAb A3C8 containing a C-terminal His-tag was used as the primary Ab (0.1 mg/mL). A mouse anti-His-tag antibody was used as the secondary Ab (1:500 dilution). An anti-mouse AP- conjugated IgG (1:500 dilution) and stabilized AP substrate were used for detection as directed.

Cell-free translation assay

Ricin biological activity was determined using a microtiter cell-free translation assay that detects luciferase translation from luciferase mRNA.[60] Dilutions of ricin are included in each assay for generation of a standard curve. Briefly, antibodies were diluted with PBS in 96-well microtiter plates. A constant amount of ricin (100 ng/mL final concentration) was added to the Ab dilutions, the plate left on a microplate shaker for 15 min (25° C), and then 5 μL was transferred to a v-shaped microtiter plate. The rabbit reticulocyte lysate, RNasin, amino acids complete, and luciferase mRNA were mixed together, and then 25 μL was added to each well. The plates were incubated (37°C) for 90 min, and then 5 μL of the translation lysate was transferred to a black microtiter plate. After the addition of the assay buffer, containing the luciferin substrate, luminescence was measured as relative light units (RLU) using a SpectraMax M5 Multi-Mode Microplate reader (Molecular Devices, LLC., Sunnyvale, CA). The average ± SD of 3 wells was reported as the percentage (%) untreated control, [(treated/untreated control) × 100].

In vitro cell cytotoxicity assay

The mouse lymphoma EL-4 cell line[61] (ATCC, Manassas, VA) was maintained in RPMI-1640 medium supplemented with 5% fetal calf serum. Immediately prior to the assay, cells were pelleted (600 × g, 10 min, 4° C) and resuspended to 2×10^6 cells/mL in RPMI-1640 medium. Using RPMI-1640 medium, sdAbs were diluted (50 μL/well) in a 96-well microtiter plate. Ricin was diluted to yield a final concentration of 200 ng/mL and was added (50 μL/well) to the antibody dilutions. After the plates had been left on a shaker for 15 min, cells (100 μL) were added to each well. The plates were incubated (37° C, 5% CO_2) overnight (17 h) after which 20 μL Cell Titer 96 was added to each well. The plate incubated for 4 additional hours. Dilutions of ricin were included in each assay and used to generate a standard curve. Optical density (490 nm) was measured on a Microplate reader. The average ± SD of 3 wells was reported as percentage (%) untreated control cells, [(OD of treated cells/OD untreated control cells) × 100].

Crystallization

SdAb A3C8 with a C-terminal His-tag (A3C8cterm) was crystallized in the ammonium sulfate grid screen condition B2 (0.1 M citric acid pH 5.0, 1.6 M ammonium sulfate) at 17°C. Protein in 50 mM Tris pH 7.6 was concentrated to 3.5 mg/mL. Hexagonal plates were obtained in hanging drops containing 1:1 mixtures of protein and precipitant.

RTA1-33/44-198 and A3C8cterm were mixed at a 1:1.1 molar ratio and was exchanged into 50 mM Tris pH 7.6, concentrated (12.5 mg/mL) and crystallized in the ammonium sulfate grid screen condition B4 (0.1 M HEPES pH 7.0, 1.6 M ammonium sulfate). Crystals grew at 17°C within a month.

X-ray crystallography

A3C8 crystals were cryo-protected in 30% glycerol, 70% ammonium sulfate grid screen condition B2. Crystals of the RTA1-33/44-198:A3C8cterm complex were cryo-protected in 30% glycerol and 70% precipitant (0.1 M HEPES pH 7.0, 1.6 M ammonium sulfate). The RTA1-33/44-198:A3C8 crystals contained 4 molecules (2 sdAb, and 2 RTA or RTA1-33/44-198 variants) per asymmetric unit.

Data were collected at 150 K using a Bruker Micro-STAR rotating anode equipped with Helios optics and a Bruker Platinum 135 CCD area detector. The structure of the complex was solved by molecular replacement using Phaser.[62] The structures of RTA (PDB 1J1M),[38] RTA1-33/44-198 (PDB 4IMV),[21] a sdAb (PDB 4FHB),[51] and the structure of the A3C8 sdAb (PDB 5SV4) were used as search models. Model-building was performed using Coot.[63,64] Simulated annealing was carried out using CNS 1.1,[65] and refinement with Refmac 5.[66,67]

Surface plasmon resonance of site-directed mutants of RTA

The dissociation constants, K_d, for each of the Abs was determined using a ProteOn™ XPR36 Protein Interaction Array System (Bio-Rad) as described previously.[68] All tests were performed on a GLC sensor chip, for general amine coupling and with a binding capacity of approximately a one protein monolayer. Following activation of the sensor chip with 0.1 M 1-ethyl-3-[3-dimethylaminopropyl]carbodiimide hydrochloride and 0.25 M N-hydroxysulfosuccinimide, immobilization was performed in 10 mM acetate buffer pH 5.0 for immobilization of RTA or its variants at 20 μg/mL on all 6 lanes. The binding kinetics of each sdAb were determined by rotating the chip and flowing various concentrations (300, 100, 33, 11, 3.7, 0 nM) over the chip at 100 μL/minute in the orthogonal direction for 90 s over the RTA-coated chip (or RTA variants) and then monitoring dissociation for 600 s using PBS with 0.005% Tween-20 (pH 7.4) or PBS with 13 mM sodium citrate (pH 4.5) as the running buffer. The surface was regenerated at 50 μL/minute with 1% phosphoric acid for 36 s. Data were corrected by subtraction of the zero antigen concentration column as well as by interspot correction.

Disclosure of potential conflicts of interest

No potential conflicts of interest were disclosed.

Funding

This work was funded by the Defense Threat Reduction Agency (DTRA) project number CBCALL12-LS6-2-0036 and the Office of Naval Research (ONR) 6.1 base funding. The opinions expressed here are those of the authors and do not represent those of the United States Department of Defense or any other agency of the United States government.

Author contributions

The manuscript was written through contributions of all authors. All authors have given approval to the final version of the manuscript.

References

1. Lanzavecchia A, Fruhwirth A, Perez L, Corti D. Antibody-guided vaccine design: identification of protective epitopes. Curr Opin Immunol 2016; 41: 62-7; PMID:27343848; http://dx.doi.org/10.1016/j.coi.2016.06.001
2. Hu X, Legler PM, Southall N, Maloney DJ, Simeonov A, Jadhav A. Structural insight into exosite binding and discovery of novel exosite inhibitors of botulinum neurotoxin serotype A through in silico screening. J Comput Aided Mol Des 2014; 28: 765-78; PMID:24958623; http://dx.doi.org/10.1007/s10822-014-9758-7
3. Maynard JA, Maassen CB, Leppla SH, Brasky K, Patterson JL, Iverson BL, Georgiou G. Protection against anthrax toxin by recombinant antibody fragments correlates with antigen affinity. Nat Biotechnol 2002; 20: 597-601; PMID:12042864; http://dx.doi.org/10.1038/nbt0602-597
4. Maddaloni M, Cooke C, Wilkinson R, Stout AV, Eng L, Pincus SH. Immunological characteristics associated with the protective efficacy of antibodies to ricin. J Immunol 2004; 172: 6221-8; PMID:15128810; http://dx.doi.org/10.4049/jimmunol.172.10.6221
5. Oswald WB, Geisbert TW, Davis KJ, Geisbert JB, Sullivan NJ, Jahrling PB, Parren PW, Burton DR. Neutralizing antibody fails to impact the course of Ebola virus infection in monkeys. PLoS Pathog 2007; 3: e9-; PMID:17238286; http://dx.doi.org/10.1371/journal.ppat.0030009
6. Audet J, Wong G, Wang H, Lu G, Gao GF, Kobinger G, Qiu X. Molecular characterization of the monoclonal antibodies composing ZMAb: a protective cocktail against Ebola virus. Sci Rep 2014; 4: 6881-; PMID:25375093; http://dx.doi.org/10.1038/srep06881
7. "HHS Select Agents and Toxins," 42 C.F.R. [§] 73.3(b) (2015)
8. Pang YP, Park JG, Wang S, Vummenthala A, Mishra RK, McLaughlin JE, Di R, Kahn JN, Tumer NE, Janosi L, et al. Small-molecule inhibitor leads of ribosome-inactivating proteins developed using the doorstop approach. PLoS One 2011; 6: e17883-; PMID:21455295; http://dx.doi.org/10.1371/journal.pone.0017883
9. Stechmann B, Bai SK, Gobbo E, Lopez R, Merer G, Pinchard S, Panigai L, Tenza D, Raposo G, Beaumelle B, et al. Inhibition of retrograde transport protects mice from lethal ricin challenge. Cell 2010; 141: 231-42; PMID:20403321; http://dx.doi.org/10.1016/j.cell.2010.01.043
10. Endo Y, Gluck A, Wool IG. Ribosomal RNA identity elements for ricin A-chain recognition and catalysis. J Mol Biol 1991; 221: 193-207; PMID:1920404; http://dx.doi.org/10.1016/0022-2836(91)80214-F
11. Olsnes S, Fernandez-Puentes C, Carrasco L, Vazquez D. Ribosome inactivation by the toxic lectins abrin and ricin. Kinetics of the enzymic activity of the toxin A-chains. Eur J Biochem 1975; 60: 281-8; PMID:1204642; http://dx.doi.org/10.1111/j.1432-1033.1975.tb21001.x
12. Audi J, Belson M, Patel M, Schier J, Osterloh J. Ricin poisoning: a comprehensive review. JAMA 2005; 294: 2342-51; PMID:16278363; http://dx.doi.org/10.1001/jama.294.18.2342
13. Wesche J. Retrograde transport of ricin. Int J Med Microbiol 2002; 291: 517-21; PMID:11890552; http://dx.doi.org/10.1078/1438-4221-00161

14. Blum JS, Fiani ML, Stahl PD. Proteolytic cleavage of ricin A chain in endosomal vesicles. Evidence for the action of endosomal proteases at both neutral and acidic pH. J Biol Chem 1991; 266: 22091-22095; PMID:1939230
15. May KL, Yan Q, Tumer NE. Targeting ricin to the ribosome. Toxicon 2013; 69: 143-51; PMID:23454625; http://dx.doi.org/10.1016/j.toxicon.2013.02.001
16. Spooner RA, Lord JM. Ricin Trafficking in Cells. Toxins (Basel) 2015; 7: 49-65; PMID:25584427; http://dx.doi.org/10.3390/toxins7010049
17. Simpson JC, Roberts LM, Romisch K, Davey J, Wolf DH, Lord JM. Ricin A chain utilises the endoplasmic reticulum-associated protein degradation pathway to enter the cytosol of yeast. FEBS Lett 1999; 459: 80-4; PMID:10508921; http://dx.doi.org/10.1016/S0014-5793(99)01222-3
18. Spooner RA, Lord JM. Ricin Trafficking in Cells. Toxins (Basel) 2015; 7: 49-65; PMID:25584427; http://dx.doi.org/10.3390/toxins7010049
19. Vitetta ES, Smallshaw JE, Schindler J. A Pilot Phase IB Clinical Trial of an Alhydrogel-Adsorbed Recombinant Ricin Vaccine (RiVax). Clin Vaccine Immunol 2012; 19(10): 1697-9; PMID:22914366; http://dx.doi.org/10.1128/CVI.00381-12
20. Pittman PR, Reisler RB, Lindsey CY, Guerena F, Rivard R, Clizbe DP, Chambers M, Norris S, Smith LA. Safety and immunogenicity of ricin vaccine, RVEc, in a Phase 1 clinical trial. Vaccine 2015; 33: 7299-306; PMID:26546259; http://dx.doi.org/10.1016/j.vaccine.2015.10.094
21. Janosi L, Compton JR, Legler PM, Steele KE, Davis JM, Matyas GR, Millard CB. Disruption of the putative vascular leak peptide sequence in the stabilized ricin vaccine candidate RTA1-33/44-198. Toxins (Basel) 2013; 5: 224-48; PMID:23364220; http://dx.doi.org/10.3390/toxins5020224
22. Rudolph MJ, Vance DJ, Cheung J, Franklin MC, Burshteyn F, Cassidy MS, Gary EN, Herrera C, Shoemaker CB, Mantis NJ. Crystal structures of ricin toxin's enzymatic subunit (RTA) in complex with neutralizing and non-neutralizing single-chain antibodies. J Mol Biol 2014; 426: 3057-68; PMID:24907552; http://dx.doi.org/10.1016/j.jmb.2014.05.026
23. Li S, Spooner RA, Allen SC, Guise CP, Ladds G, Schnoder T, Schmitt MJ, Lord JM, Roberts LM. Folding-competent and folding-defective forms of ricin A chain have different fates after retrotranslocation from the endoplasmic reticulum. Mol Biol Cell 2010; 21: 2543-54; PMID:20519439; http://dx.doi.org/10.1091/mbc.E09-08-0743
24. Eijsink VG, Bjork A, Gaseidnes S, Sirevag R, Synstad B, van den BB, Vriend G. Rational engineering of enzyme stability. J Biotechnol 2004; 113: 105-20; PMID:15380651; http://dx.doi.org/10.1016/j.jbiotec.2004.03.026
25. Eijsink VG, Gaseidnes S, Borchert TV, van den BB. Directed evolution of enzyme stability. Biomol Eng 2005; 22: 21-30; PMID:15857780; http://dx.doi.org/10.1016/j.bioeng.2004.12.003
26. Mansfeld J, Vriend G, Dijkstra BW, Veltman OR, van den BB, Venema G, Ulbrich-Hofmann R, Eijsink VG. Extreme stabilization of a thermolysin-like protease by an engineered disulfide bond. J Biol Chem 1997; 272: 11152-6; PMID:9111013; http://dx.doi.org/10.1074/jbc.272.17.11152
27. Vriend G, Berendsen HJ, van den BB, Venema G, Eijsink VG. Early steps in the unfolding of thermolysin-like proteases. J Biol Chem 1998; 273: 35074-7; PMID:9857041; http://dx.doi.org/10.1074/jbc.273.52.35074
28. Pace CN, Shirley BA, Thomson JA. A Practical Approach (The Practical Approach Series), 2nd Edition, Oxford University Press (May 18, 1989); 311-30; ISBN-10: 0199630003 ISBN-13: 978-0199630004.
29. Argent RH, Parrott AM, Day PJ, Roberts LM, Stockley PG, Lord JM, Radford SE. Ribosome-mediated folding of partially unfolded ricin A-chain. J Biol Chem 2000; 275: 9263-9; PMID:10734065; http://dx.doi.org/10.1074/jbc.275.13.9263
30. Compton JR, Legler PM, Clingan BV, Olson MA, Millard CB. Introduction of a disulfide bond leads to stabilization and crystallization of a ricin immunogen. Proteins 2011; 79: 1048-60; PMID:21387408; http://dx.doi.org/10.1002/prot.22933
31. Zabetakis D, Olson MA, Anderson GP, Legler PM, Goldman ER. Evaluation of disulfide bond position to enhance the thermal stability of a highly stable single domain antibody. PLoS ONE 2014; 9: e115405-; PMID:25526640; http://dx.doi.org/10.1371/journal.pone.0115405
32. Argent RH, Roberts LM, Wales R, Robertus JD, Lord JM. Introduction of a disulfide bond into ricin A chain decreases the cytotoxicity of the ricin holotoxin. J Biol Chem 1994; 269: 26705-10; PMID:7929403
33. Anderson GP, Liu JL, Hale ML, Bernstein RD, Moore M, Swain MD, Goldman ER. Development of antiricin single domain antibodies toward detection and therapeutic reagents. Anal Chem 2008; 80: 9604-11; PMID:19072267; http://dx.doi.org/10.1021/ac8019398
34. Goldman ER, Liu JL, Bernstein RD, Swain MD, Mitchell SQ, Anderson GP. Ricin detection using phage displayed single domain antibodies. Sensors (Basel) 2009; 9: 542-55; PMID:22389616; http://dx.doi.org/10.3390/s90100542
35. Turner KB, Liu JL, Zabetakis D, Lee AB, Anderson GP, Goldman ER. Improving the biophysical properties of anti-ricin single-domain antibodies. 2015; 6: 27-35; http://dx.doi.org/10.1016/j.btre.2015.01.001
36. Vance DJ, Mantis NJ. Resolution of two overlapping neutralizing B cell epitopes within a solvent exposed, immunodominant alpha-helix in ricin toxin's enzymatic subunit. Toxicon 2012; 60: 874-7; PMID:22750533; http://dx.doi.org/10.1016/j.toxicon.2012.06.014
37. Olson MA, Carra JH, Roxas-Duncan V, Wannemacher RW, Smith LA, Millard CB. Finding a new vaccine in the ricin protein fold. Protein Eng Des Sel 2004; 17: 391-397; PMID:15187223; http://dx.doi.org/10.1093/protein/gzh043
38. Watanabe K, Motoshima H. Ricin A-chain (Recombinant) at 100K, PDB 1J1M. 2009; http://dx.doi.org/10.2210/pdb1J1M/pdb
39. George J, Compton JR, Leary DH, Olson MA, Legler PM. Structural and mutational analysis of a monomeric and dimeric form of a single domain antibody with implications for protein misfolding. Proteins 2014; PMID:25136772; http://dx.doi.org/10.1002/prot.24671
40. Legler PM, Brey RN, Smallshaw JE, Vitetta ES, Millard CB. Structure of RiVax: a recombinant ricin vaccine. Acta Crystallogr D Biol Crystallogr 2011; 67: 826-30; PMID:21904036; http://dx.doi.org/10.1107/S0907444911026771
41. Song K, Mize RR, Marrero L, Corti M, Kirk JM, Pincus SH. Antibody to ricin a chain hinders intracellular routing of toxin and protects cells even after toxin has been internalized. PLoS ONE 2013; 8: e62417-; PMID:23638075; http://dx.doi.org/10.1371/journal.pone.0062417
42. Pincus SH, Das A, Song K, Maresh GA, Corti M, Berry J. Role of Fc in antibody-mediated protection from ricin toxin. Toxins (Basel) 2014; 6: 1512-25; PMID:24811206; http://dx.doi.org/10.3390/toxins6051512
43. Colombatti M, Pezzini A, Colombatti A. Monoclonal antibodies against ricin: effects on toxin function. Hybridoma 1986; 5: 9-19; PMID:3957360; http://dx.doi.org/10.1089/hyb.1986.5.9
44. Pincus SH, Das A, Song K, Maresh GA, Corti M, Berry J. Role of Fc in antibody-mediated protection from ricin toxin. Toxins (Basel) 2014; 6: 1512-25; PMID:24811206; http://dx.doi.org/10.3390/toxins6051512
45. McConnell AD, Zhang X, Macomber JL, Chau B, Sheffer JC, Rahmanian S, Hare E, Spasojevic V, Horlick RA, King DJ, et al. A general approach to antibody thermostabilization. MAbs 2014; 6: 1274-82; PMID:25517312; http://dx.doi.org/10.4161/mabs.29680
46. McConnell AD, Spasojevich V, Macomber JL, Krapf IP, Chen A, Sheffer JC, Berkebile A, Horlick RA, Neben S, King DJ, et al. An integrated approach to extreme thermostabilization and affinity maturation of an antibody. Protein Eng Des Sel 2013; 26: 151-64; PMID:23173178; http://dx.doi.org/10.1093/protein/gzs090
47. Lord JM, Spooner RA. Ricin trafficking in plant and mammalian cells. Toxins (Basel) 2011; 3: 787-801; PMID:22069740; http://dx.doi.org/10.3390/toxins3070787
48. Chia PZ, Gleeson PA. The regulation of endosome-to-Golgi retrograde transport by tethers and scaffolds. Traffic 2011; 12: 939-47; PMID:21477175; http://dx.doi.org/10.1111/j.1600-0854.2011.01185.x
49. Carra JH, McHugh CA, Mulligan S, Machiesky LM, Soares AS, Millard CB. Fragment-based identification of determinants of conformational and spectroscopic change at the ricin active site. BMC Struct Biol 2007; 7: 72-; PMID:17986339; http://dx.doi.org/10.1186/1472-6807-7-72
50. Yan X, Hollis T, Svinth M, Day P, Monzingo AF, Milne GW, Robertus JD. Structure-based identification of a ricin inhibitor. J Mol Biol 1997; 266: 1043-9; PMID:9086280; http://dx.doi.org/10.1006/jmbi.1996.0865

51. Oyen D, Wechselberger R, Srinivasan V, Steyaert J, Barlow JN. Mechanistic analysis of allosteric and non-allosteric effects arising from nanobody binding to two epitopes of the dihydrofolate reductase of Escherichia coli. Biochim Biophys Acta 2013; 1834: 2147-57; PMID:23911607; http://dx.doi.org/10.1016/j.bbapap.2013.07.010
52. Fong RH, Banik SS, Mattia K, Barnes T, Tucker D, Liss N, Lu K, Selvarajah S, Srinivasan S, Mabila M, et al. Exposure of epitope residues on the outer face of the chikungunya virus envelope trimer determines antibody neutralizing efficacy. J Virol 2014; 88: 14364-79; PMID:25275138; http://dx.doi.org/10.1128/JVI.01943-14
53. Porta J, Jose J, Roehrig JT, Blair CD, Kuhn RJ, Rossmann MG. Locking and blocking the viral landscape of an alphavirus with neutralizing antibodies. J Virol 2014; 88: 9616-23; PMID:24920796; http://dx.doi.org/10.1128/JVI.01286-14
54. Moskaug JO, Sandvig K, Olsnes S. Cell-mediated reduction of the interfragment disulfide in nicked diphtheria toxin. A new system to study toxin entry at low pH. J Biol Chem 1987; 262: 10339-45; PMID:3112141
55. Lazear E, Whitbeck JC, Ponce-de-Leon M, Cairns TM, Willis SH, Zuo Y, Krummenacher C, Cohen GH, Eisenberg RJ. Antibody-induced conformational changes in herpes simplex virus glycoprotein gD reveal new targets for virus neutralization. J Virol 2012; 86: 1563-76; PMID:22130533; http://dx.doi.org/10.1128/JVI.06480-11
56. Turner KB, Liu JL, Zabetakis D, Lee AB, Anderson GP, Goldman ER. Improving the biophysical properties of anti-ricin single-domain antibodies. Biotechnology Reports 2015; 6: 27-35; http://dx.doi.org/10.1016/j.btre.2015.01.001
57. Vance DJ, Tremblay JM, Mantis NJ, Shoemaker CB. Stepwise engineering of heterodimeric single domain camelid VHH antibodies that passively protect mice from ricin toxin. J Biol Chem 2013; 288: 36538-47; PMID:24202178; http://dx.doi.org/10.1074/jbc.M113.519207
58. Graef RR, Anderson GP, Doyle KA, Zabetakis D, Sutton FN, Liu JL, Serrano-Gonzalez J, Goldman ER, Cooper LA. Isolation of a highly thermal stable lama single domain antibody specific for Staphylococcus aureus enterotoxin B. BMC Biotechnol 2011; 11: 86-; PMID:21933444; http://dx.doi.org/10.1186/1472-6750-11-86
59. Zabetakis D, Anderson GP, Bayya N, Goldman ER. Contributions of the complementarity determining regions to the thermal stability of a single-domain antibody. PLoS ONE 2013; 8: e77678-; PMID:24143255; http://dx.doi.org/10.1371/journal.pone.0077678
60. Hale ML. Microtiter-based assay for evaluating the biological activity of ribosome-inactivating proteins. Pharmacol Toxicol 2001; 88: 255-60; PMID:11393586; http://dx.doi.org/10.1111/j.1600-0773.2001.880506.x
61. van HT, van BJ, van Veelen PA, Kraakman M, Heukamp LC, Koning F, Melief CJ, Ossendorp F, Offringa R. Identification of a novel tumor-specific CTL epitope presented by RMA, EL-4, and MBL-2 lymphomas reveals their common origin. J Immunol 2000; 165: 869-77; PMID:10878361; http://dx.doi.org/10.4049/jimmunol.165.2.869
62. McCoy AJ, Grosse-Kunstleve RW, Adams PD, Winn MD, Storoni LC, Read RJ. Phaser crystallographic software. J Appl Crystallogr 2007; 40: 658-74; PMID:19461840; http://dx.doi.org/10.1107/S0021889807021206
63. Emsley P, Cowtan K. Coot: model-building tools for molecular graphics. Acta Crystallogr D Biol Crystallogr 2004; 60: 2126-32; PMID:15572765; http://dx.doi.org/10.1107/S0907444904019158
64. Emsley P, Lohkamp B, Scott WG, Cowtan K. Features and development of Coot. Acta Crystallogr D Biol Crystallogr 2010; 66: 486-501; PMID:20383002; http://dx.doi.org/10.1107/S0907444910007493
65. Brünger AT, Adams PD, Clore GM, DeLano WL, Gros P, Grosse-Kunstleve RW, Jiang JS, Kuszewski J, Nilges M, Pannu NS, et al. Crystallography & NMR system: A new software suite for macromolecular structure determination. Acta Crystallogr D Biol Crystallogr 1998; 54: 905-21; PMID:9757107; http://dx.doi.org/10.1107/S0907444998003254
66. Collaborative Computational Project N4. The CCP4 suite: programs for protein crystallography. Acta Crystallogr D Biol Crystallogr 1994; 50: 760-3; PMID:15299374; http://dx.doi.org/10.1107/S0907444994003112
67. Painter J, Merritt EA. Optimal description of a protein structure in terms of multiple groups undergoing TLS motion. Acta Crystallogr D Biol Crystallogr 2006; 62: 439-50; PMID:16552146; http://dx.doi.org/10.1107/S0907444906005270
68. Anderson GP, Legler PM, Zabetakis D, Goldman ER. Comparison of immunoreactivity of staphylococcal enterotoxin B mutants for use as toxin surrogates. Anal Chem 2012; 84: 5198-5203; PMID:22681495; http://dx.doi.org/10.1021/ac300864j
69. Rutenber E, Katzin BJ, Ernst S, Collins EJ, Mlsna D, Ready MP, Robertus JD. Crystallographic refinement of ricin to 2.5 A. Proteins 1991; 10: 240-250; PMID:1881880; http://dx.doi.org/10.1002/prot.340100308
70. Legler PM, Brey RN, Smallshaw JE, Vitetta ES, Millard CB. Structure of RiVax: a recombinant ricin vaccine. Acta Crystallogr D Biol Crystallogr 2011; 67: 826-30; PMID:21904036; http://dx.doi.org/10.1107/S0907444911026771
71. Lemley PV, Amanatides P, Wright DC. Identification and characterization of a monoclonal antibody that neutralizes ricin toxicity in vitro and in vivo. Hybridoma 1994; 13: 417-21; PMID:7860097; http://dx.doi.org/10.1089/hyb.1994.13.417
72. Lebeda FJ, Olson MA. Prediction of a conserved, neutralizing epitope in ribosome-inactivating proteins. Int J Biol Macromol 1999; 24: 19-26; PMID:10077268; http://dx.doi.org/10.1016/S0141-8130(98)00059-2
73. Castelletti D, Fracasso G, Righetti S, Tridente G, Schnell R, Engert A, Colombatti M. A dominant linear B-cell epitope of ricin A-chain is the target of a neutralizing antibody response in Hodgkin's lymphoma patients treated with an anti-CD25 immunotoxin. Clin Exp Immunol 2004; 136: 365-72; PMID:15086403; http://dx.doi.org/10.1111/j.1365-2249.2004.02442.x
74. Castelletti D, Colombatti M. Peptide analogues of a T-cell epitope of ricin toxin A-chain prevent agonist-mediated human T-cell response. Int Immunol 2005; 17: 365-72; PMID:15724064; http://dx.doi.org/10.1093/intimm/dxh216